Thermoacoustic Thermal Management for Electric Aircraft

Luis A. Rodriguez¹, Rodger W. Dyson², Mark P. Wernet³, Ronald J. Leibach⁴

NASA Glenn Research Center, Cleveland, OH, 44035, USA

Electric aircraft research and development is on the rise, necessitating an avant-garde thermal management system to effectively dissipate and reuse the typically wasted low-grade thermal energy generated on electric aircraft. Hence, the Thermal Recovery Exergy Efficient System (TREES) was successfully modeled, designed, built, and tested at NASA Glenn Research Center (NASA GRC) to demonstrate a solution. TREES demonstrates the ability to transport and amplify acoustic energy over various distances, with minimal energy dissipation, while creating a thermoacoustic heat pump that can deliver and absorb thermal energy. The inhouse rig is now being utilized as a diagnostics testbed to understand the underlying physics of traveling wave thermoacoustics and to enhance future thermal management technology development.

I. Nomenclature

TREES = Thermal Recovery Exergy Efficient System

TMS = Thermal Management
TAHP = Thermoacoustic Heat Pump
ACT = Advanced Cooling Technologies

HX = Heat Exchanger SS = Stainless Steel

 ΔT = Temperature Difference

LM = Linear Motor

 T_h = Hot side temperature, K T_c = Cold side temperature, K

II. Introduction

Electrification research of air vehicles is a burgeoning field that is becoming increasingly complex as the need for megawatt power levels increases [1,2]. These high-power levels generate large heat loads which must be rejected to maintain an optimal operating temperature for all components. The challenges posed to stable TMS operation are dependent on several factors, such as high heat loads from electrical components and limited surface area of the aircraft for heat dissipation. Additionally, weight minimization of the thermal management system is needed to prevent further energetic losses. Current thermal management solutions have major disadvantages such as added weight, low thermal capacity, and no increase of exergy [3]. Table 1 contains the current approaches to managing dissipated thermal energy and their disadvantages. Inefficient TMS can lead to overheating of components, reduce system efficiency, and potential safety hazards. Therefore, developing innovative and effective thermal management architecture/infrastructure is crucial for the successful implementation of TMS systems within an electric aircraft.

¹ Space and Aeronautics Research Engineer, Thermal Energy Conversion Branch, and AIAA Member.

² Hybrid Gas Electric Propulsion Technical Lead, Thermal Energy Conversion Branch, and AIAA Member.

³Senior Research Engineer, Optics and Photonics Branch, AIAA Associate Fellow

⁴Research Engineer, Thermal Energy Conversion Branch, AIAA Member

TREES was developed as a novel approach that may solve the disadvantages of the current TMS technologies [3]. A full-scale sized aircraft TREES system can harness the high-grade waste heat, that is wasted by fully electric or hybrid electric aircraft, and convert it to acoustic energy via entry stages called thermal amplifiers [4]. Sources of high and low-grade heat are shown in Figure 1. This system will operate by first converting the incoming thermal energy into acoustic energy. Subsequently, the acoustic energy is channeled through a network of tubes leading to acoustic heat pumps. Within the heat pumps, the acoustic energy converts back to low-grade thermal energy. Finally, the low-grade heat from the acoustic pump can be distributed and reused throughout the aircraft via a solid-state heat pipe network [5,6]. The solid-state waste heat delivery system will be used to manage the thermal energy transfer to critical applications such as de-icing, local skin heating, thrust augmentation, fuel preheating, and aircraft environment control. Mass estimates for an aircraft sized TMS have not been determined, but ideas of embedding TREES into an aircraft structure may be possible.

A TAHP system has been developed between ACT and NASA GRC for an aircraft sized TMS and cooling of a 1 MW solid-state DC circuit breaker [6]. This system contains 6 stages to simulate locations where heat sources can discharge their thermal energy and a heat pump stage for cooling of the circuit breaker. Initial, models show that the ACT TAHP can handle up to 7.5 kW of waste heat input. The purpose of this work is to show and describe how the GRC proof-of-concept demonstration contributed to the larger scale ACT TREES build and test. Therefore, this paper describes the initial modeling, design, fabrication, and testing of an in-house traveling wave thermoacoustic testbed. Current GRC testbed designs are meant to handle up to 800 Ws of high-grade waste heat, demonstrate acoustic energy amplification, and be utilized as a diagnostic toolset for new TAHP designs that required higher loads of high-grade waste heat.

Table 1. Present Thermal Management Solutions

Thermal Management Technology	Disadvantage	
Ram air HX	Adds weight, aircraft drag, displaces fuel capacity	
Convective skin cooling HX	Adds weight, drag, and requires liquid pumping losses	
Sinking heat into fuel	Limited thermal capacity due to coking and volume	
Sinking heat into lubricating oil	Limited thermal capacity, Low delta T adds HX mass	
Active cooling	Reduces propulsive efficiency, Adds weight and maintenance	
Phase change cooling	Limited thermal capacity, Adds weight	
Heat Pipe, Pumped Multiphase	Does not increase Exergy which impacts mass and efficiency	

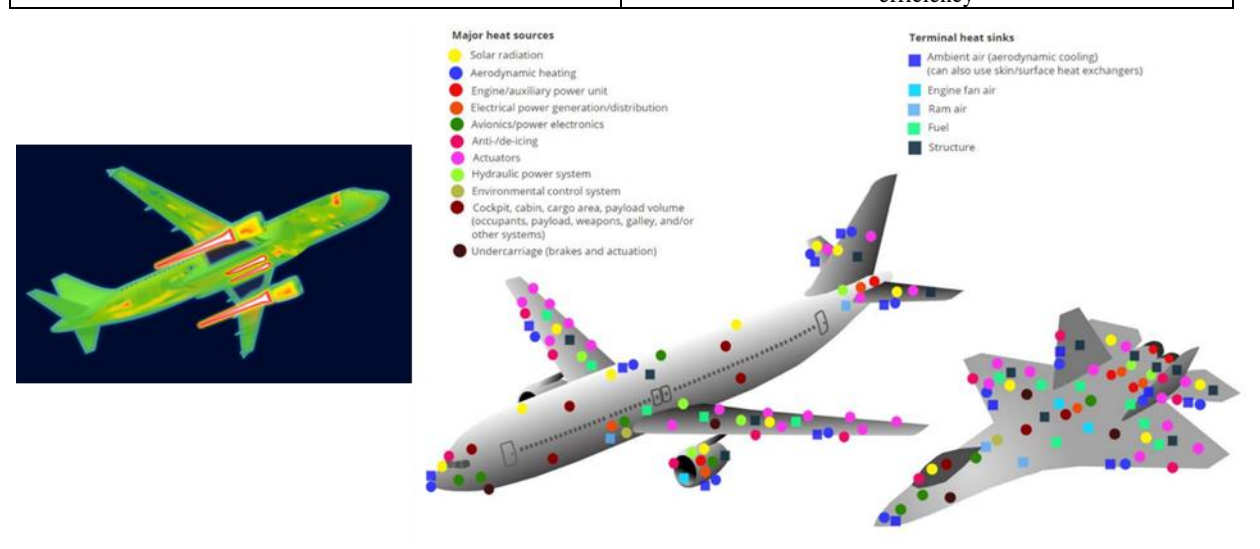


Figure 1. Sources of High and Low-Grade Wasted Heat and Heat Sinks [3,7]

III. Thermoacoustic Traveling Wave Concepts

In the thermoacoustic domain, two main types of waves exist: standing and traveling. Early developments of the thermoacoustic phenomena were investigated by Sondhauss [8] in 1850. Standing wave systems were one of the first systems to convert acoustic energy to thermal energy at low efficiencies. Traveling waves, investigated by Ceperley in 1979 [9], were introduced to overcome standing wave inefficiencies. In his study, he concluded that the phase correlation between the velocity and pressure in the regenerator of Stirling systems was fairly similar to that observed in a traveling wave system. The crucial concept behind Stirling and traveling wave systems is that as the gas oscillates within the regenerator it experiences thermal compression when the pressure is low and thermal expansion when the pressure is high. Also, within the regenerator, the velocity of the oscillating gas along the regenerator's temperature gradient is in phase with the pressure [10]. Achieving optimal thermal contact between the gas and the regenerator materials is essential for acoustic power to develop. In contrast, a standing wave device requires that the thermal contact between the gas and the stack be carefully balanced, ensuring it is neither too weak nor too strong. For a traveling wave system, the synergy between oscillating gas and the regenerator ensures that all the work is occurring within the regenerator every cycle.

A traveling wave device is reversible, meaning that it can work as a heat engine and as a heat pump. The heat engine can be combined with the heat pump to amplify the heat lifted by the pump. An example system architecture of an amplified heat pump with heat flow between the oscillating gas parcels and the regenerator wall is shown in Figure 2. In this simplified image, the gas parcels are oscillating horizontally, and each position of the parcel describes the direction of heat flow between the parcel and regenerator walls. Volumetric changes due to the expansion and compression cycles are also shown. Separate gas parcel illustrations are shown for both the heat engine and heat pump. Important aspects for inducing optimal amplification and heat pumping in a TREES environment are absolute temperature ratio (Th/Tc), frequency, and proper phasing between pressure and velocity within the regenerator. To acquire phasing in the regenerator the system geometry must be optimized to obtain the proper compliance, inertance, and resistance in the thermoacoustic network. [3, 10-11].

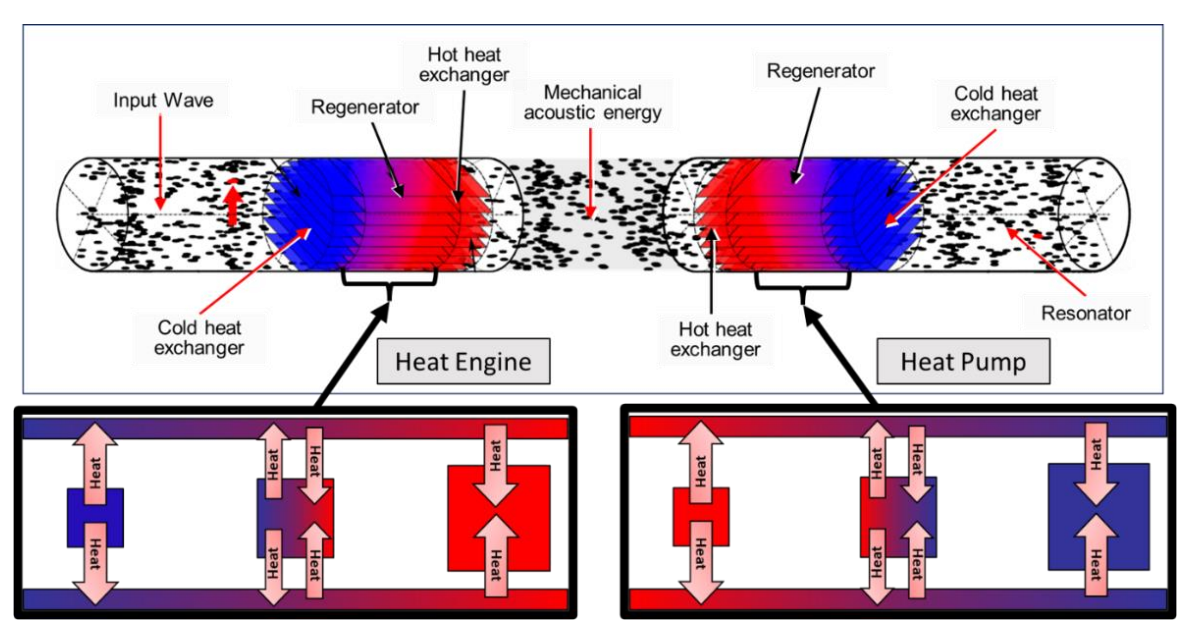


Figure 2. Combination of Heat Engine and Heat Pump Along with Gas Parcel Volumetric Change and Heat Flow Direction [3]

IV. TREES Sage Modeling and Design

Sage is a one-dimensional object-oriented commercial software package used for modeling and optimizing Stirling convertors and is one of the most accurate Stirling convertor modeling programs in use by NASA GRC. This code is the successor to GLIMPS (Globally Implicit Stirling Cycle Simulation), and GLOP (GLIMPS Optimization) software created by Gedeon Associates. Model input parameters are typically physical geometry, material/gas type, temperatures, frequency, charge pressure, and number of time/space nodes. Sage is typically used to model Stirling

convertors, Stirling cryocoolers, and thermoacoustic heat pump/engines. The software has also been used by NASA and partners to aid in design optimization. In addition, Sage is also capable of modeling electromagnetic components such as linear alternators and controllers.

The TREES Sage model is based on Sage's "InLinePTR" example [12], which assumes a single-stage pulse-tube cooler in-line with the regenerator. Figure 3 illustrates a physical representation of the in-line PTR model and Figure 4 demonstrates the same model in Sage form. In this paper, the TREES Sage model was modified for the development of an in-house experimental framework. An optimal design was reached by optimizing for the heat lifted by the heat pump.

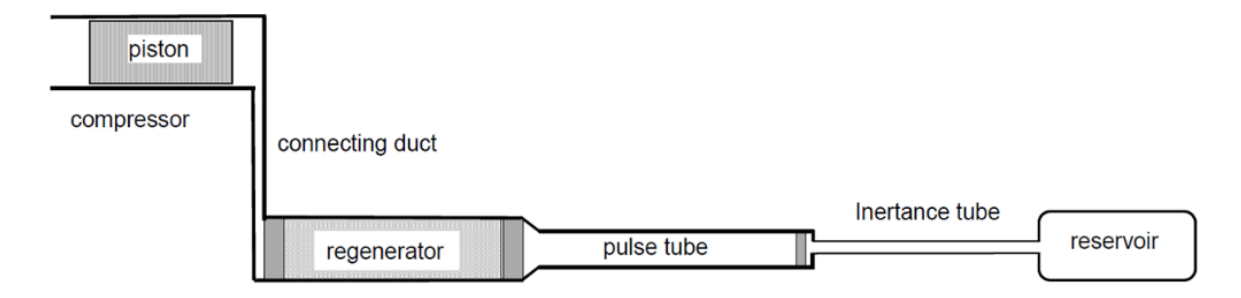


Figure 3. Schematic of Physical Model from "InLinePTR" [12]

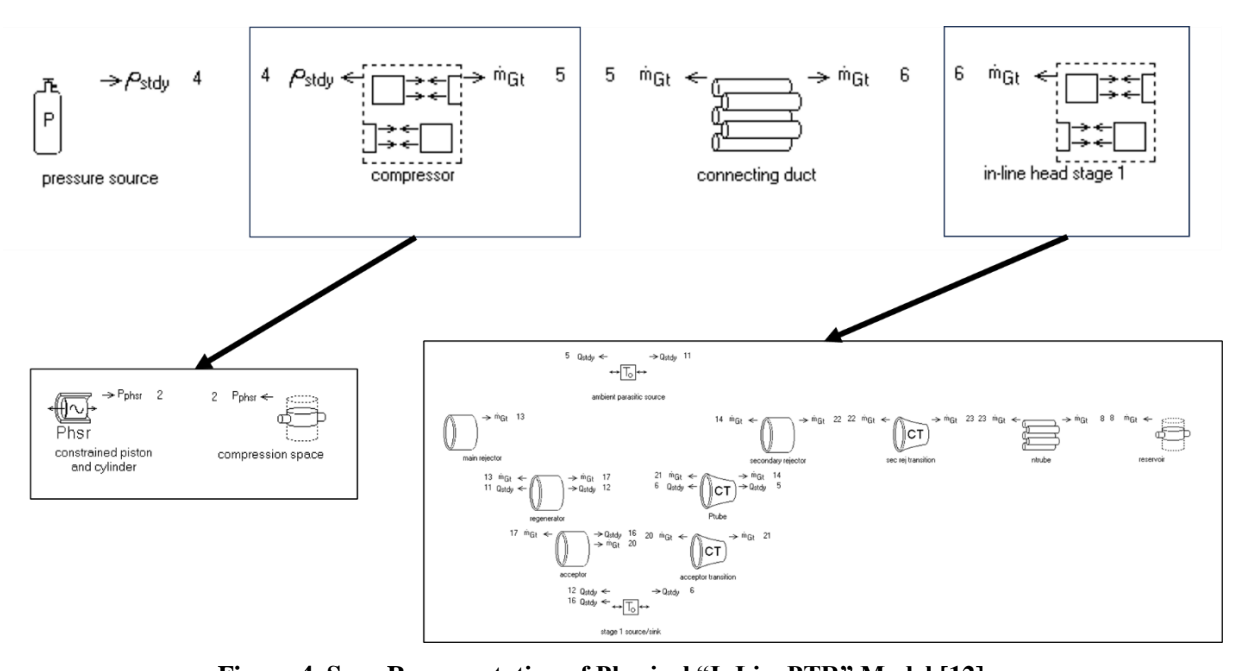


Figure 4. Sage Representation of Physical "InLinePTR" Model [12]

V. Experimental Set Up

A. TREES 1.0: Low Power System Design and Hardware

A schematic of the TAHP components is shown in Figure 5, which contains similar components to the Sage represented model. The instrumentation for monitoring system operation and performance of the TAHP is shown in Figure 6. With in the blue box labeled "Heat Pump" a regenerator composed of SS meshed discs is sandwiched between two copper heat exchangers. The rig consists of various thermocouples sensors to measure temperature variation along the assembly. Thermocouple density is the highest along the heat pump to capture an accurate

temperature gradient between the cold and hot side heat exchangers. Accelerometers are used for the purpose of capturing unusual vibrations such as piston over-stroke. The pressure sensors on the schematic are used to ensure similar pressure readings on opposite sides of the rig. The mean working pressure of TREES is 3 MPa. A power feedthrough, also shown in the instrumental schematic, provides power to the LM, which induces the acoustic wave. A programable AC source, Chroma model 61602, is used to supply voltage and current to the LM. Furthermore, National Instruments data acquisition modules are used to acquire real-time sensor data using LabVIEW software, which also controls the LM.

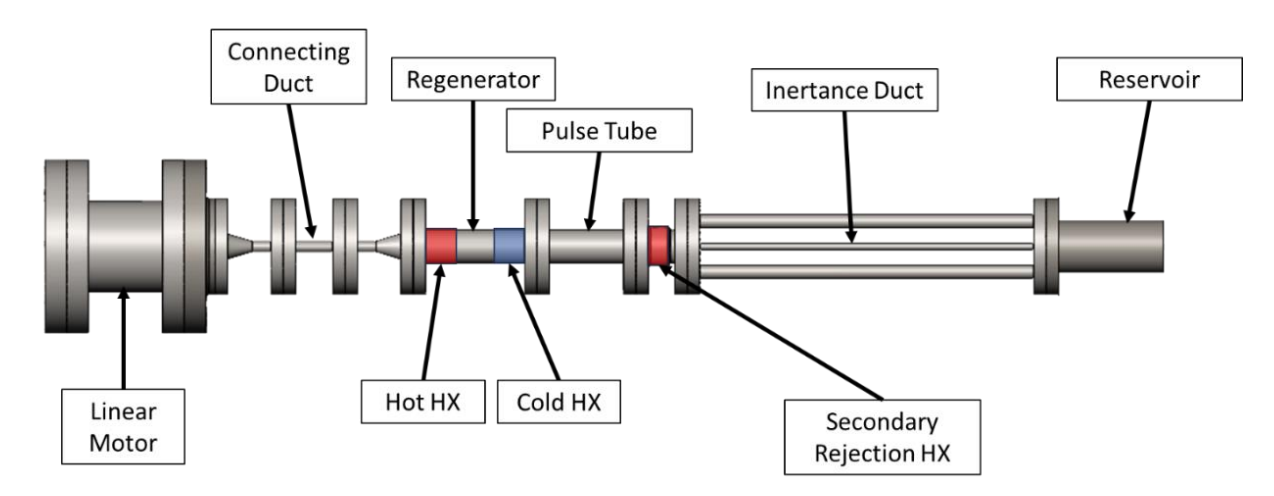


Figure 5. TAHP System Components

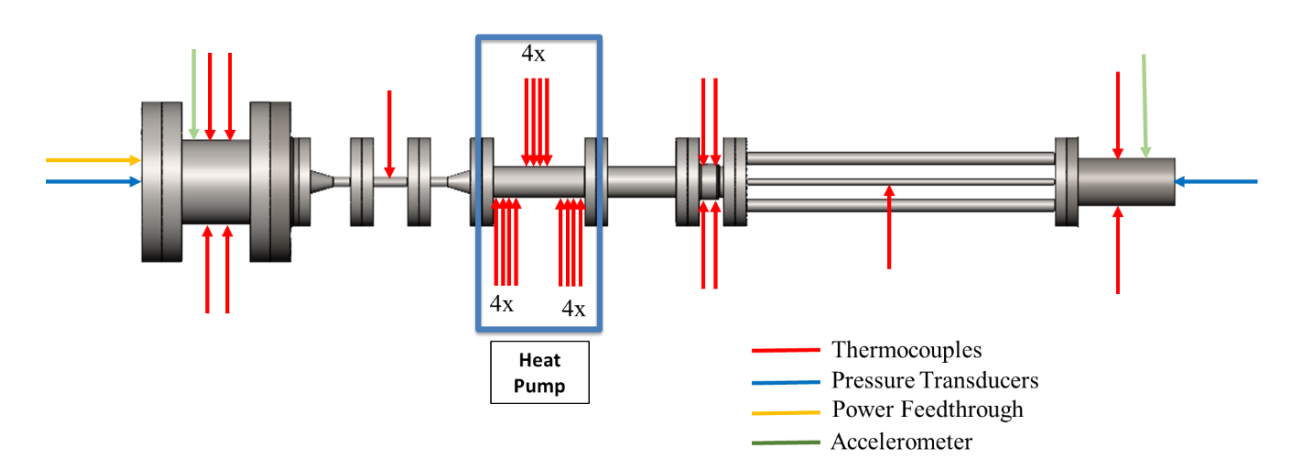


Figure 6. Instrumentation Set Up for Low Heat Lift Rig

A campaign of experimental tests is conducted to stablish a baseline for future higher power acoustic configurations. The length of the connecting duct was varied from 0.2 m, 5 m, to 10 m as shown inside the blue boxes, detailed by their respective length, in Figure 7. A length of 10 m is comparable to the length of a private jet. Helical ducts were created for the 5 m and 10 m lengths to conserve room on the test stand. Varying connecting duct length will assist in determining a maximum length where the onset of significant acoustic energy dissipation occurs. An image of the in-lab rig is shown in Figure 8. Two 5 m helical ducts are tested for further investigation on the degradation of acoustic energy. One contains a 90-degree elbow transition and the second has a smooth transition as shown in Figure 9 in (a) and (b) respectively. These two 5 m helical ducts were later used to build up a 10 m connecting duct.

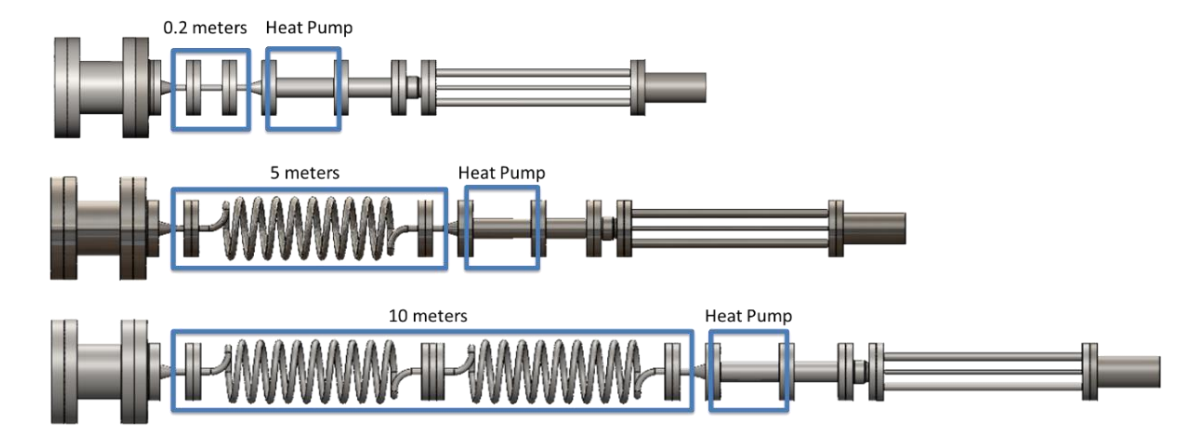


Figure 7. Connecting Duct Lengths of TAHP and Heat Pump Location

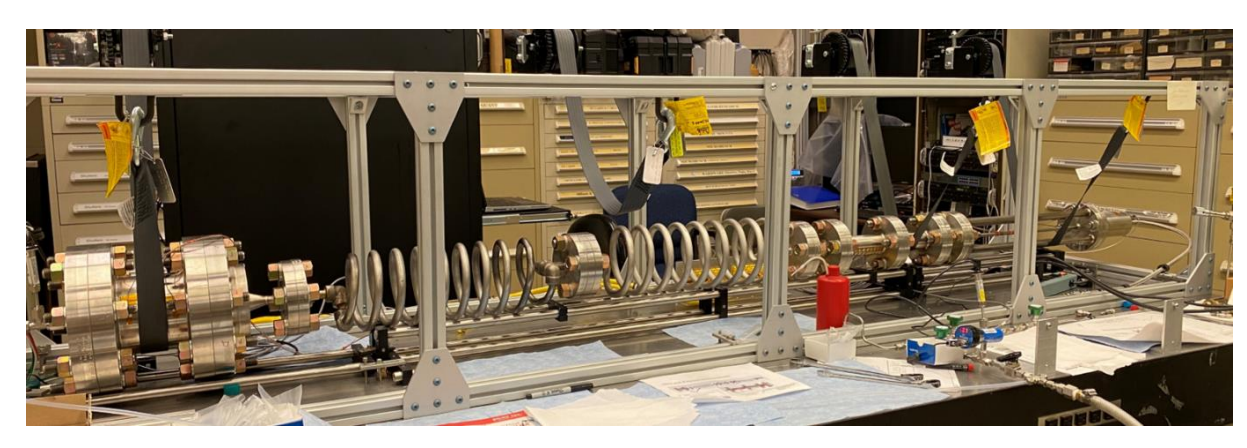
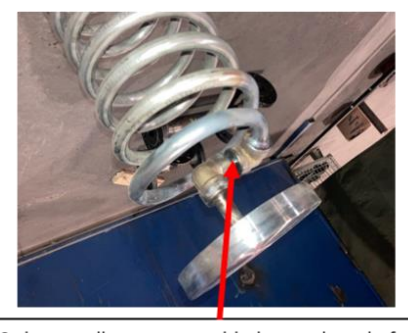


Figure 8. In-Lab TAHP with 10 Meter Connecting Duct



(a): 90-degree elbows were added at each end of the helical tube component



(b) : No 90-degree elbows on the 2nd iteration of helical tube component

Figure 9. Two Types of 5 Meter Connecting Ducts (a) 90-Degree Elbow and (b) Smooth Transition

B. TREES 2.0: Addition of Thermal Amplifier for Acoustic Power Amplification

An update to the previous TAHP was modeled, designed, and manufactured to amplify the acoustic energy delivered from the LM. The addition to the previous TAHP design is bounded by the red dashed lines and illustrated in Figure 10. A thermal amplifier, which can also be called a heat engine, is part of the newly added section. Additional thermocouples and heat flux sensors were added to acquire a more definitive temperature distribution and to capture

heat flux data so that it can be compared to the Sage modeling prediction. The updated instrumentation architecture can be seen in Figure 11. Analogous to the heat pump, the amplifier is composed of a cold HX, a hot HX, and finally a regenerator is sandwiched in between both HXs. The cold HX of the amplifier is cooled by a 75 KW Neslab chiller, which cools the housing surface of the SS to 17°C. The hot side HX is heated using a ceramic heater band, raising the heating surface temperature to 500°C.

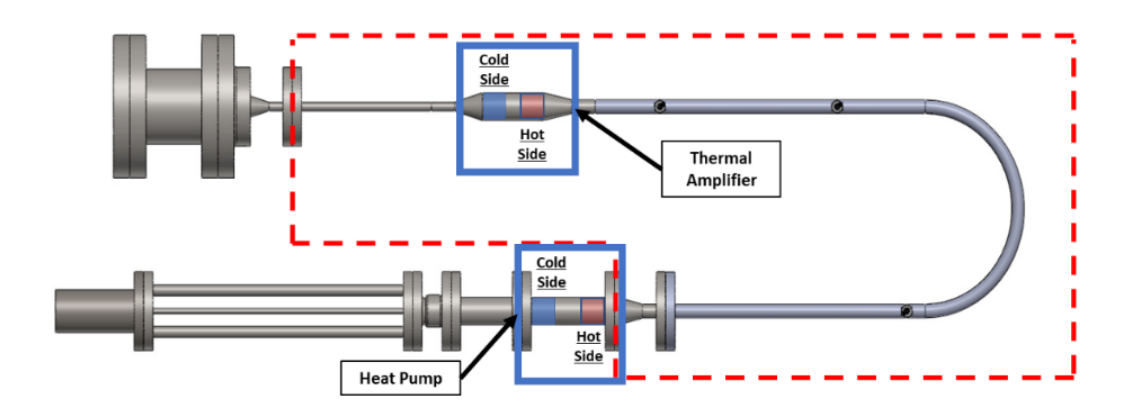


Figure 10. Thermal Amplifier Addition

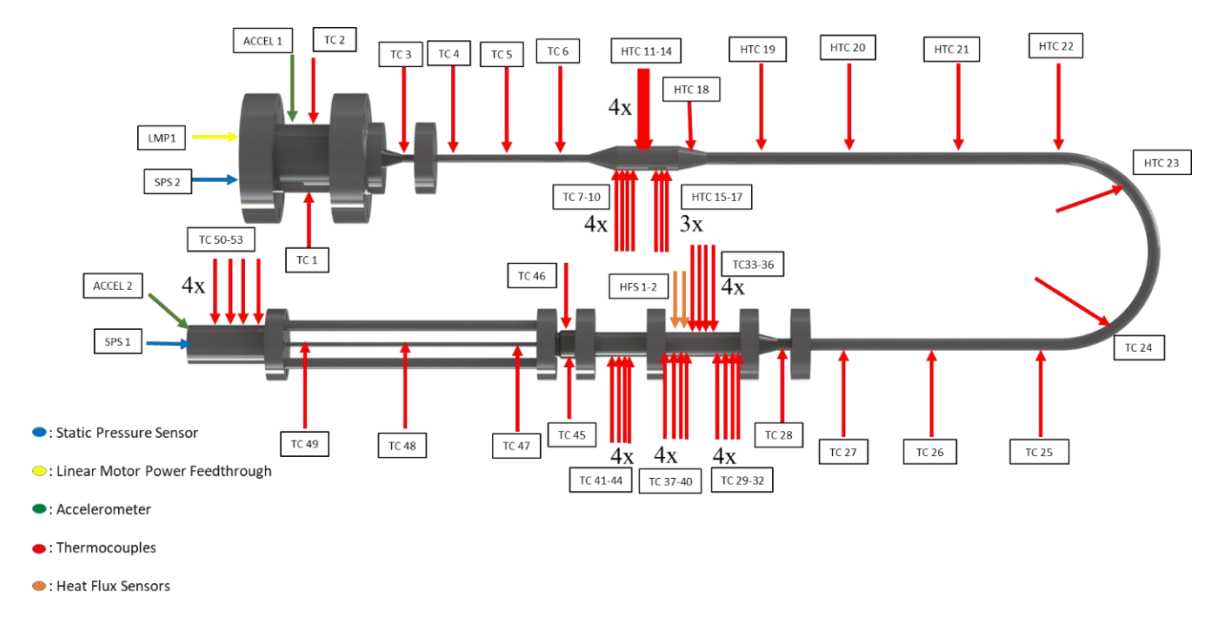


Figure 11. Instrumented Thermally Amplified Rig

C. Optical Spool and Schlieren Method

TAHP systems operate at high pressures using a pure gas charge, which makes probing these systems very challenging. The linear motor generates pressure waves, which can be measured using pressure sensors. However, there is little information known about the velocity fields inside of TAHP systems. In order to gain insight on the state of the gas inside the TAHP, a Self-Aligned Focusing Schlieren system is used to study the convective flow velocities inside of the TAHP [13]. The objective of the diagnostic investigation is to understand the relative phasing of the velocity fields inside TAHP versus the pressure fields. SAFS data is collected using a Photron high speed camera combined with a Cavilux pulsed laser system operating at 6kHz and 30 ns pulse widths. The TAHP uses a mechanically driven piston to generate acoustic waves (@60Hz) inside of a 50 mm ID tube connected to a regenerator to provide heating and/or cooling. Optical access for the SA-FS system is obtained by fabricating an optical spool piece to fit into the TAHP system. In order to withstand the pressure differential of 3 MPa, a nominally 32 mm thick

window is required to ensure a sufficient margin of safety. Making the inside surface of the window curved to match the 50 mm tubing ID results in a strong lensing effect. Instead, a fused quartz glass tube with 50 mm ID and 1mm thick walls is used to match the inside ID of the TAHP system tubing, see Figure 12. A 32 mm thick plane window is designed into the housing with an air gap between the outside of the glass tube and the inside surface of the plane window. The airspace between the outside of the 1 mm thick cylindrical tube and the inside of the plane window is plumbed to be in equilibrium with the Helium gas within the TAHP. Hence, the 1 mm thick glass cylinder yields minimal refractions while the 32mm thick plane parallel window withstands the large pressure differential without imparting additional refractions. The optical spool is positioned after the heat pump, where thermocouples 41-44 are shown in Figure 12.

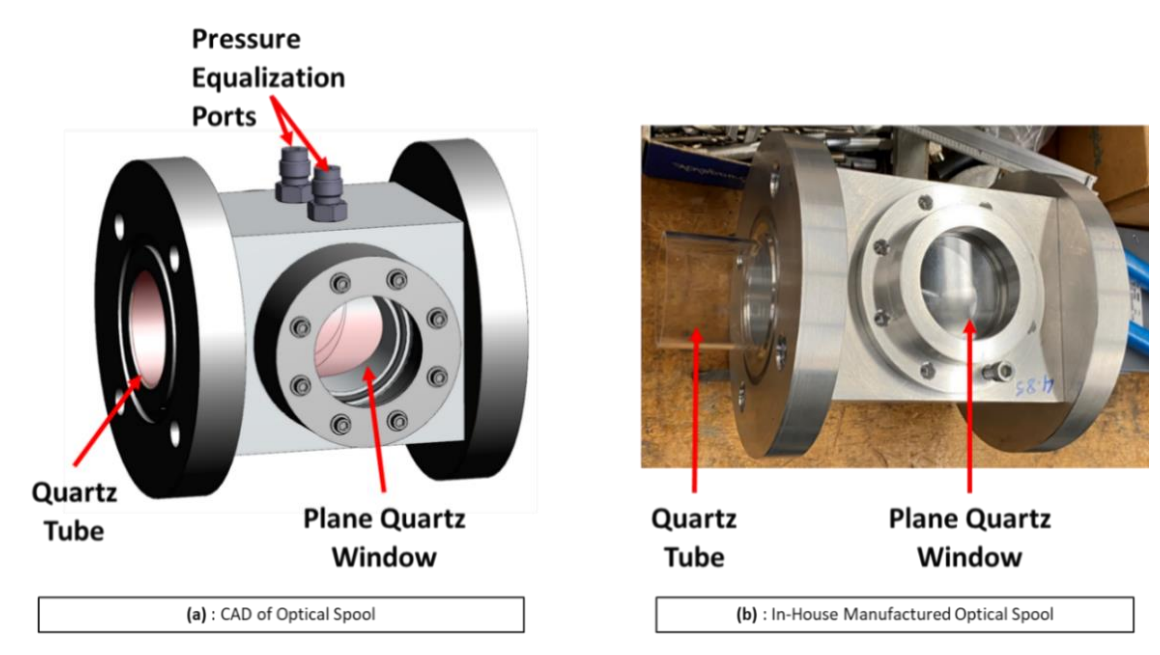


Figure 12. Optical Spool (a) CAD and (b) In-House Build

VI. Results and Analysis

A. TREES 1.0: Low Power TAHP

Results for the 0.2m, 5m, and 10m tests are shown in Figures 13-16, where the rig operating temperatures are plotted from startup. Each plot displays the temperature profiles for the hot side HX, cold side HX, and regenerator. The temperature profiles also demonstrate a working heat pump as a result of the traveling wave thermoacoustic effects. Before the LM is turned on, all curves follow a similar temperature trend around 21 °C but soon diverge after the LM is energized. Thermocouple measurements show thermoacoustic pumping of heat out of the cold HX and into the hot side HX, see Figure 2 for reference. Although it may appear self-evident, it is worth noting that this phenomenon is characterized by the initial relative decrease in temperature of the cold HX and the corresponding increase in temperature of the hot HX. Time duration for each connecting duct length test was kept similar to illustrate the max ΔT differences between the hot and cold HXs.

Table 2 tabulates the results from each duct length configuration along with each respective ΔT . The table contains duct length, maximum temperature from hot HX, minimum temperature from cold HX, and the difference between maximum and minimum temperatures. Temperature ΔTs show that the 5 m duct with the 90° elbows has the lowest ΔT , which signifies a source of acoustic power loss. Therefore, when both 5 m ducts are assembled together to form a 10 m length acoustic degradation is also observed due to both the 90° transition and duct length. The smooth transition 5m duct exhibited only a small drop in performance compared to the 0.2m length duct.

Thermocouple temperature data from the 10 m test were used as inputs to a COMSOL Multiphysics® thermal simulation of the 10 m rig to calculate the heat lifted from the cold side of the heat pump. COMSOL's heat transfer

module is used along with surface integration tool to capture the thermal energy results. The heat lifted is compared to the Sage model in Figure 17. Although Sage predicts a higher heat lift, the experimental/COMSOL results are within an expected range. Future work will involve calibration of Sage models over a range of test data for accurate predictions. An IR camera was also used to record the temperature profile along the regenerator, where pieces of black tape were placed over the thermocouples to provide estimates of the underlying SS surface temperature.

Table 2. Connecting Duct Length and Temperature Difference Between Respective Maximum and Minimum Temperatures

Connecting Duct Length (m)	Maximum Temperature (°C)	Minimum Temperature (°C)	ΔT (°C)
0.2	50.83	16.42	34.42
5 (90° Elbow)	47.62	18.06	29.56
5 (Smooth)	51.53	18.56	32.97
10	48.38	19.53	28.85

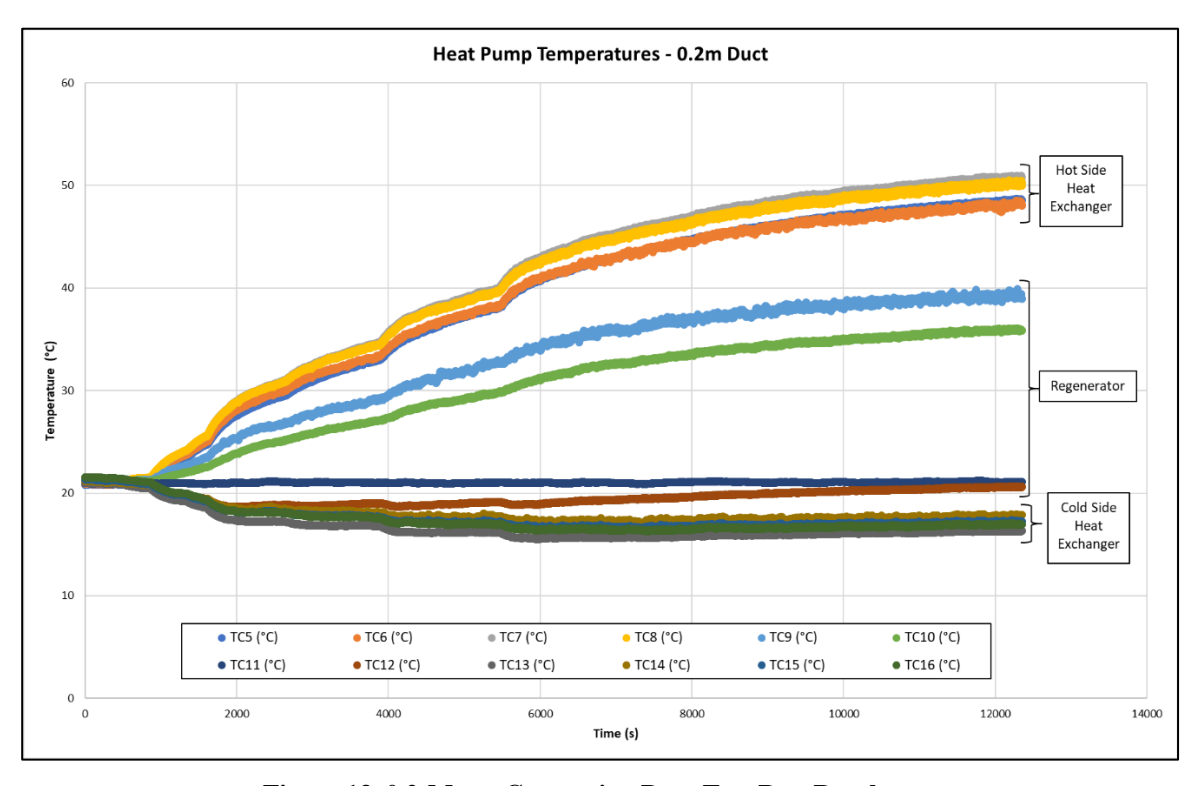


Figure 13. 0.2-Meter Connecting Duct Test Run Results

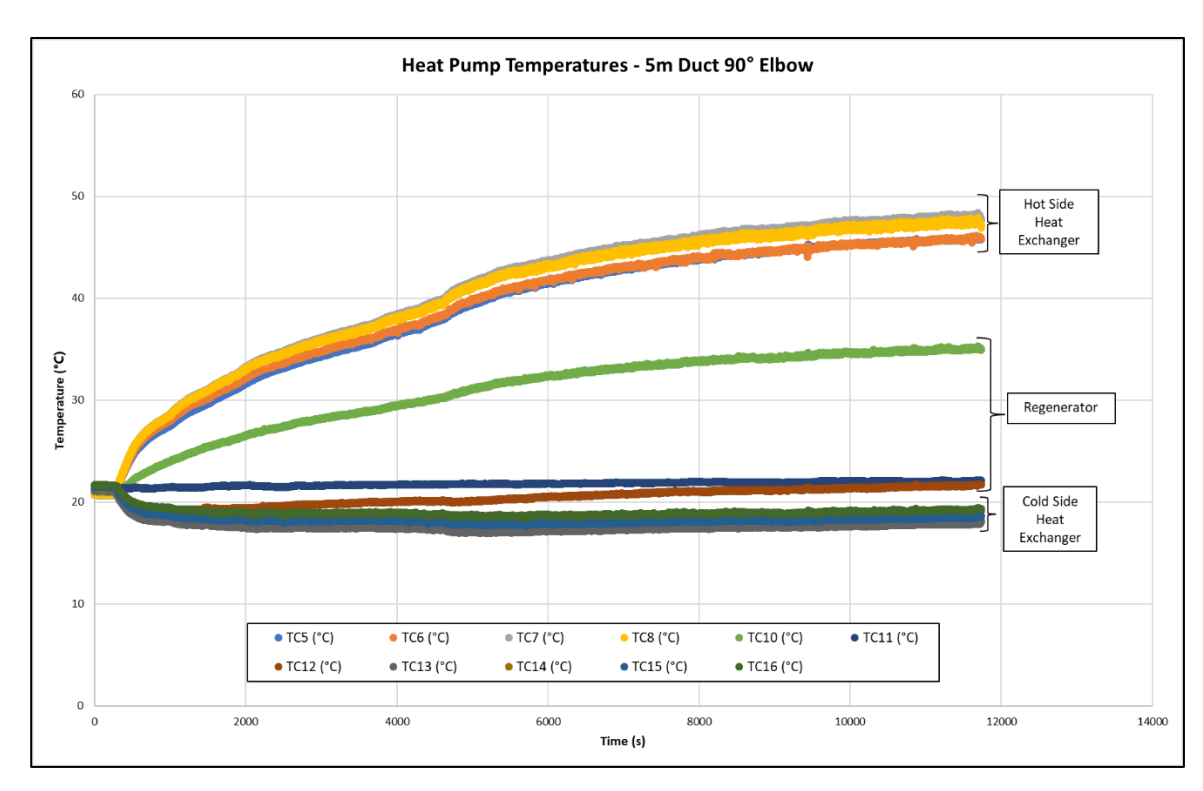


Figure 14. 5-Meter 90-Degree Elbow Transition Connecting Duct Test Run Results

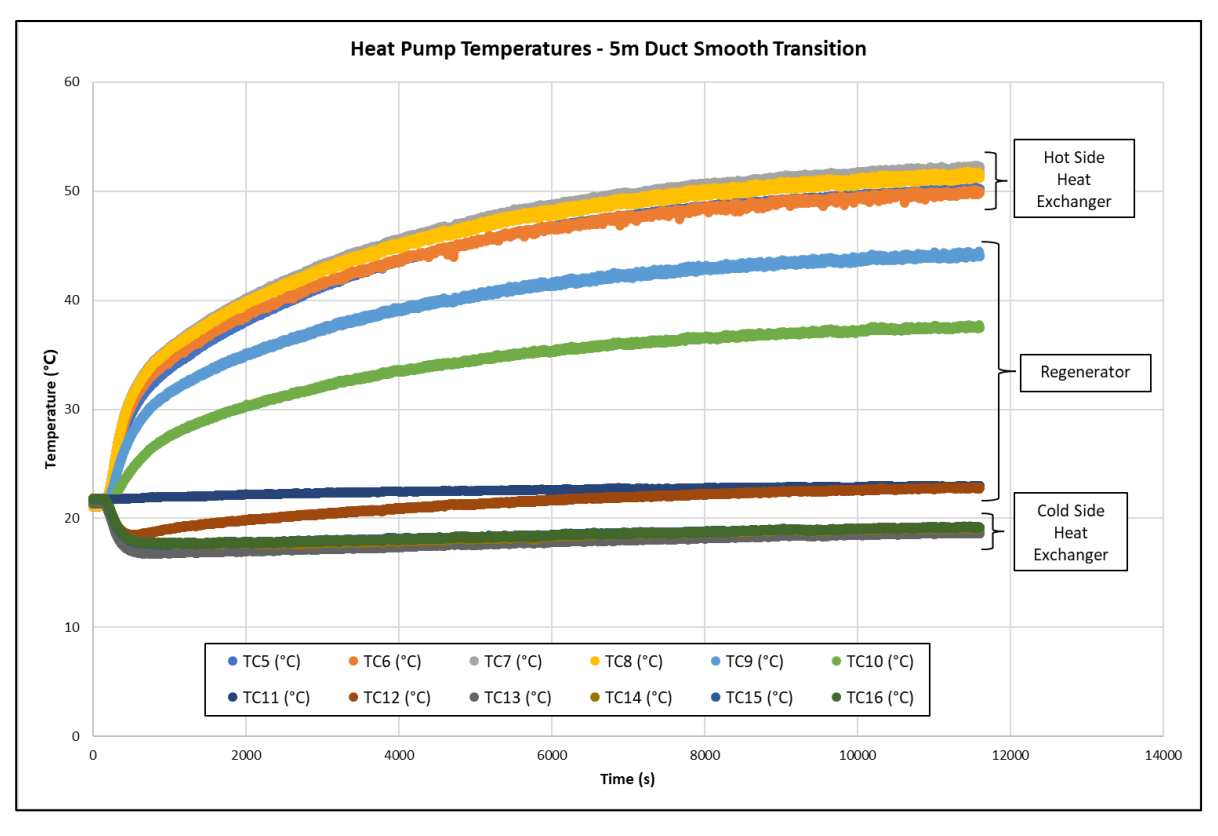


Figure 15. 5-Meter Smooth Transition Connecting Duct Test Run Results

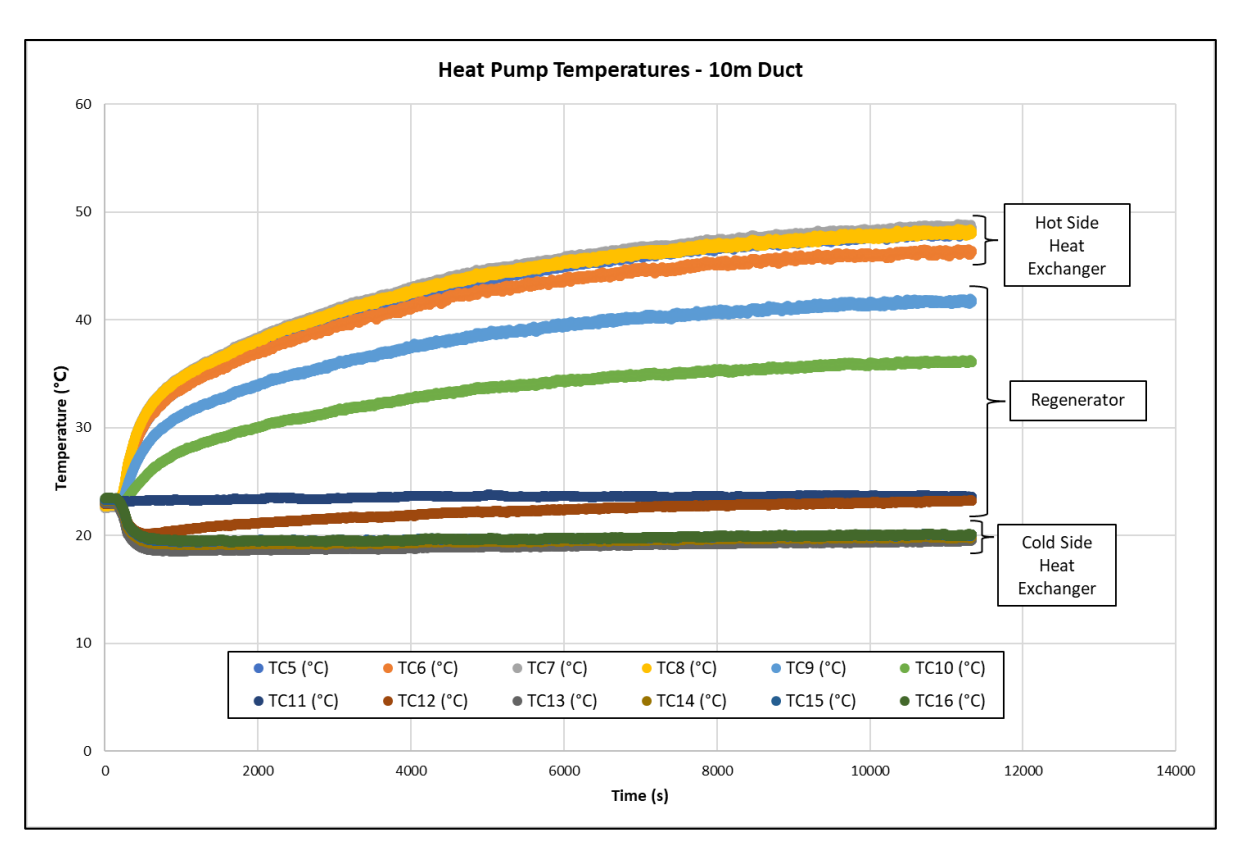


Figure 16. 10-Meter Connecting Duct Test Run Results

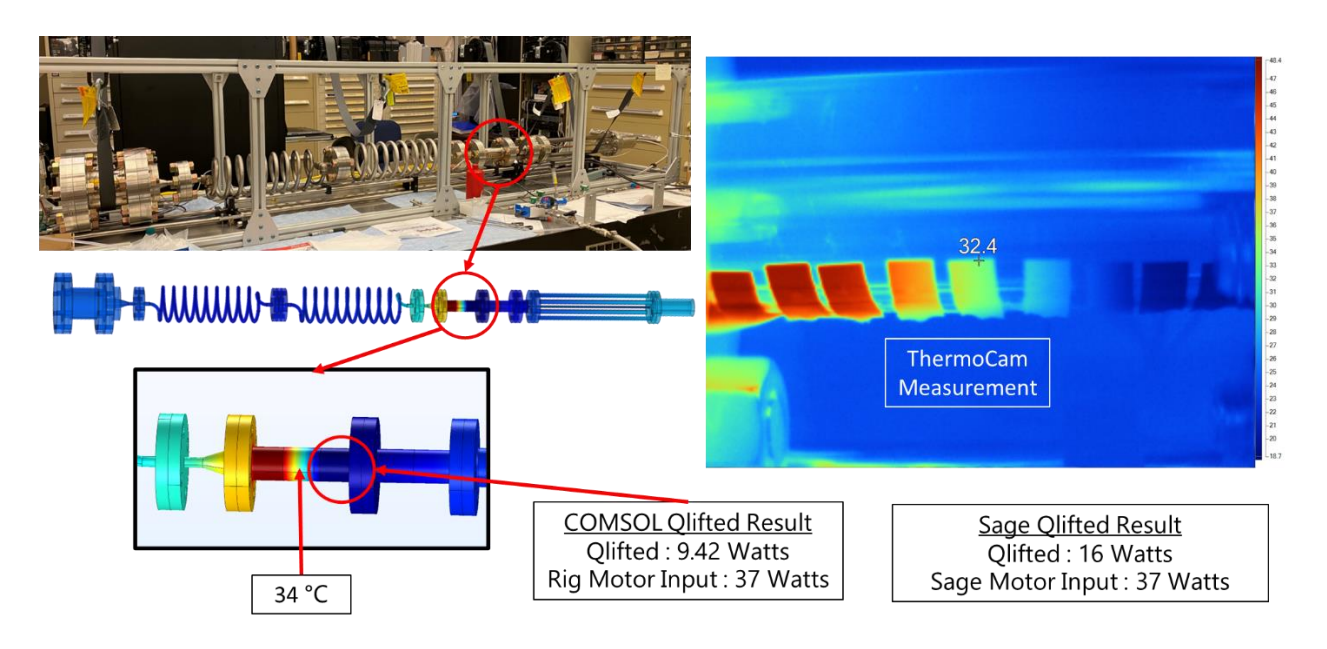


Figure 17. COMSOL, Sage, and ThermoCam Data Comparison

B. TREES 2.0: Acoustic Power Amplification of TAHP

An acoustic amplifier, or heat engine, was integrated into TREES 1.0 to increase the heat pump's ΔT . As a result of earlier testing and experimentation, two different test cases were devised for the improved design: one at maximum hot side engine temperature (500°C) and the other at maximum power input from the LM. Current limits for both tests

are set at 3.5 Arms, which are based on the motor limit of 4 A_{rms} . Thermocouple measurements of the maximum temperature tests for the heat engine and heat pump are shown in Figure 18 and Figure 19, respectfully. Table 3 details Δ Ts for both the heat engine and heat pump. Initially, when powering the LM, no thermal loads are applied to the heat engine. This leads to a heat pump like behavior within the thermal amplifier as shown in Figure 18. When the amplifier is heat pumping the hot side becomes the cold side and the cold side become the hot side. Once the thermal loads are applied, acoustic power amplification is observed between the 1400-1500 s into the run. This event causes a temperature reversal around the 1500 s region.

Figure 19 illustrates how the heat pump temperature distribution is affected by the thermal amplifier. Similar to the heat engine, in the 1500 s region, an inflection in temperature is observed for all thermocouples. This change in curvature signifies an augmentation in acoustic power. The onset for amplification can also be described by the LM's voltage and current data shown in Figure 20. As previously stated, to stay within safe bounds of testing, a maximum current limit of 3.5 A_{rms} was chosen. During the initial phase of testing, when the amplifier is working as a heat pump, the current limit is reached at ~530 s. Once amplification is underway, a sudden drop in current occurs at ~1500 s, while voltage remains quasi-steady between 27 and 30 V_{rms} . The decrease in current most likely implies that the oscillating piston in the LM is required to do less work, indicating less power is required to the motor and amplification is occurring as a result of the thermal load differential being applied to the heat engine.

Table 3. Maximum Temperature Test: Maximum Temperature, Minimum Temperature, and ΔT for Heat Engine and Heat Pump Components

TREES Component	Maximum Temperature (°C)	Minimum Temperature (°C)	ΔT (°C)
Heat Engine	509.15	17.03	492.12
Heat Pump	87.28	19.52	67.77

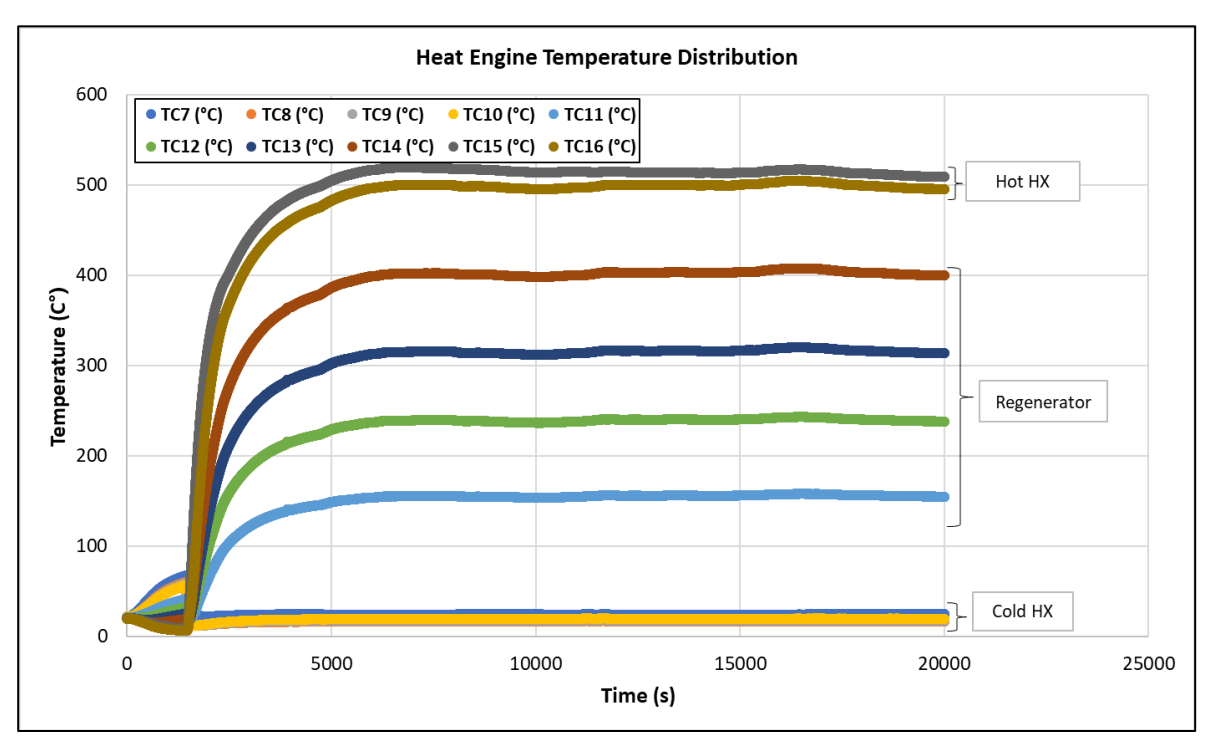


Figure 18. Heat Engine Maximum Temperature Thermocouple Data

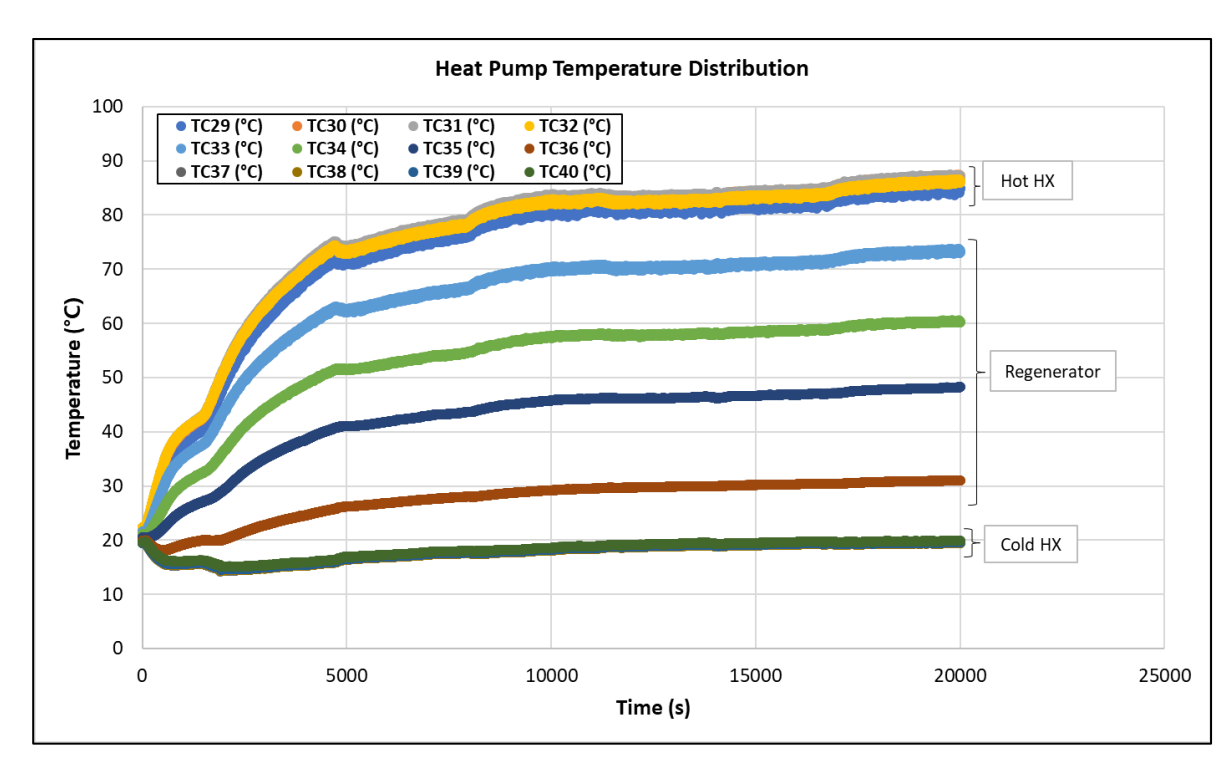


Figure 19. Heat Pump Maximum Temperature Thermocouple Data

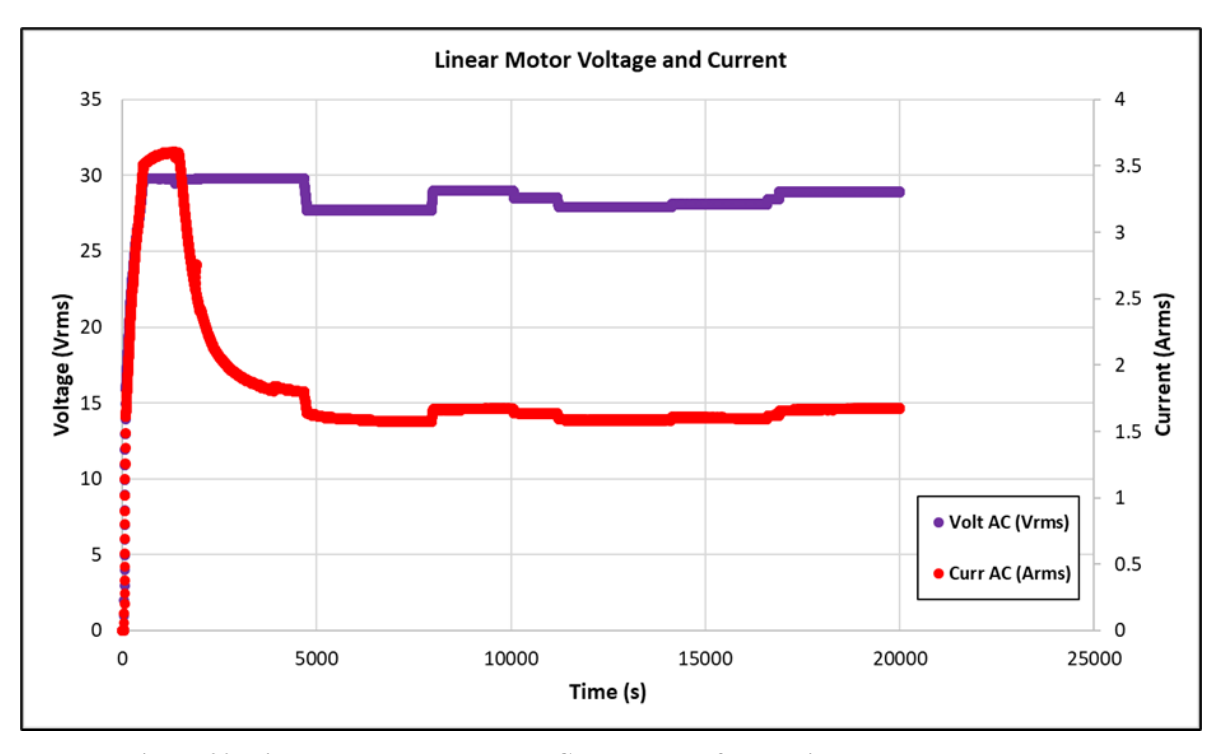


Figure 20. Linear Motor Voltage and Current Data for Maximum Temperature Test

Comparable attributes are shown in Figure 21 and Figure 22, with respect to the maximum temperature test plots for the heat engine and heat pump. The amplifiers heat pump behavior is shown, the onset of amplification occurs between the $1400-1500 \, \text{s}$, and a temperature reversal occurs at $\sim 1500 \, \text{s}$. The objective of driving the LM with a high-

power input from the Chroma power source, while respecting current limits, is twofold: first, to achieve steady-state conditions for all thermocouple readings in the heat pump, and second, to maximize the ΔT while trying to achieve 500°C temperature on the hot side of the heat engine. Although, the heat pump, reached steady-state conditions at ~15000 s and the ΔT doubled with respect to the previous maximum temperature test, a 500°C temperature was not attained. The highest temperature that could be reached on heat engine's hot side while driving the LM at maximum power input was 408°C. Temperature data plots for both the heat engine and heat pump are shown in Figure 21 and Figure 22, respectively. Table 4 specifies relevant temperatures and ΔTs for both the heat engine and heat pump. The reason that 500°C is not reachable is likely the result of the net heat removal occurring within the amplification section. When driving the LM by increasing voltage and respecting current limits, the piston amplitude is also being increased and thus increasing the acoustic power that is delivered into the system. Voltage and current data are shown in Figure 23. Simultaneously, as the acoustic power continues to be amplified, the intake of thermal energy into the hot heat exchanger is also amplified by the traveling wave. Therefore, the voltage increase results in additional thermal power needed by the wave from the heater band to maintain a stable 500°C temperature. A COMSOL and Sage evaluation was not performed for the amplification study.

Table 4. Maximum Input Power Test: Maximum Temperature, Minimum Temperature, and ΔT for Heat Engine and Heat Pump Components

TREES Component	Maximum Temperature (°C)	Minimum Temperature (°C)	ΔT (°C)
Heat Engine	408.77	16.88	391.89
Heat Pump	145.94	24.35	124.59

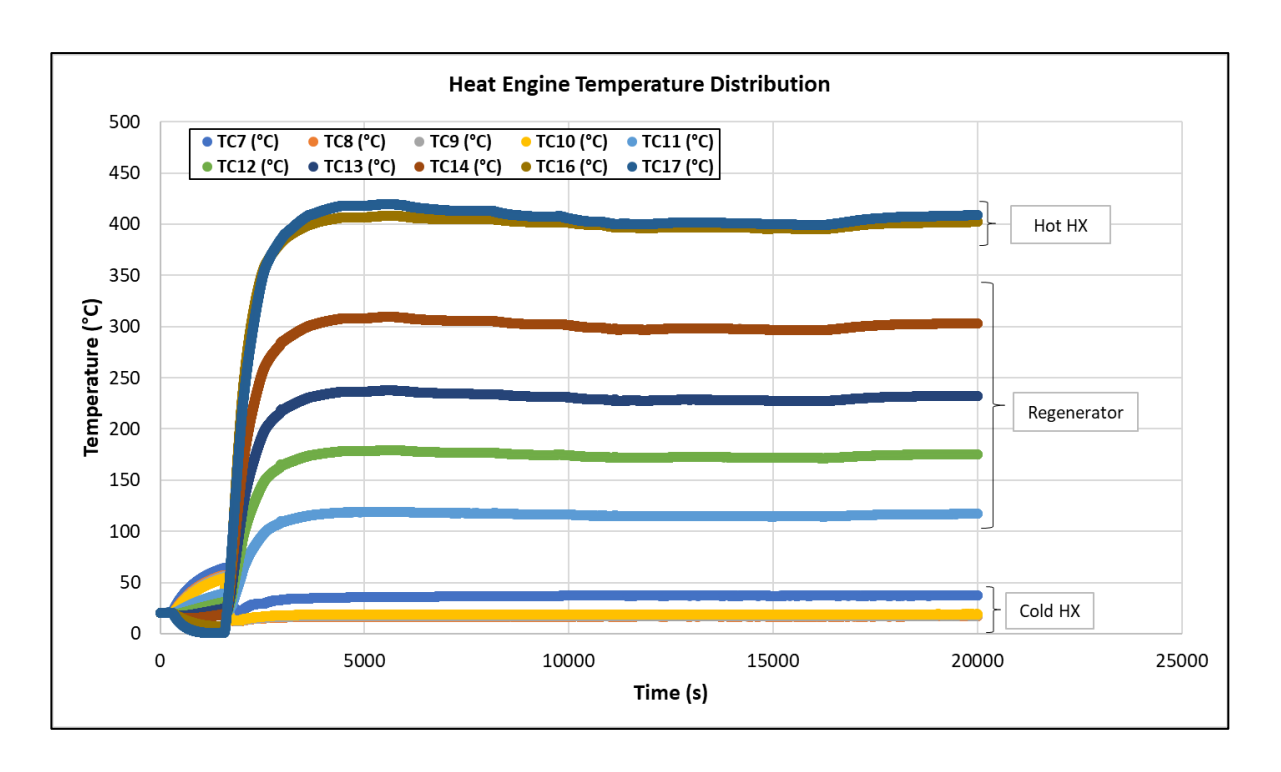


Figure 21. Heat Engine Maximum Power Input From Alternator Thermocouple Data

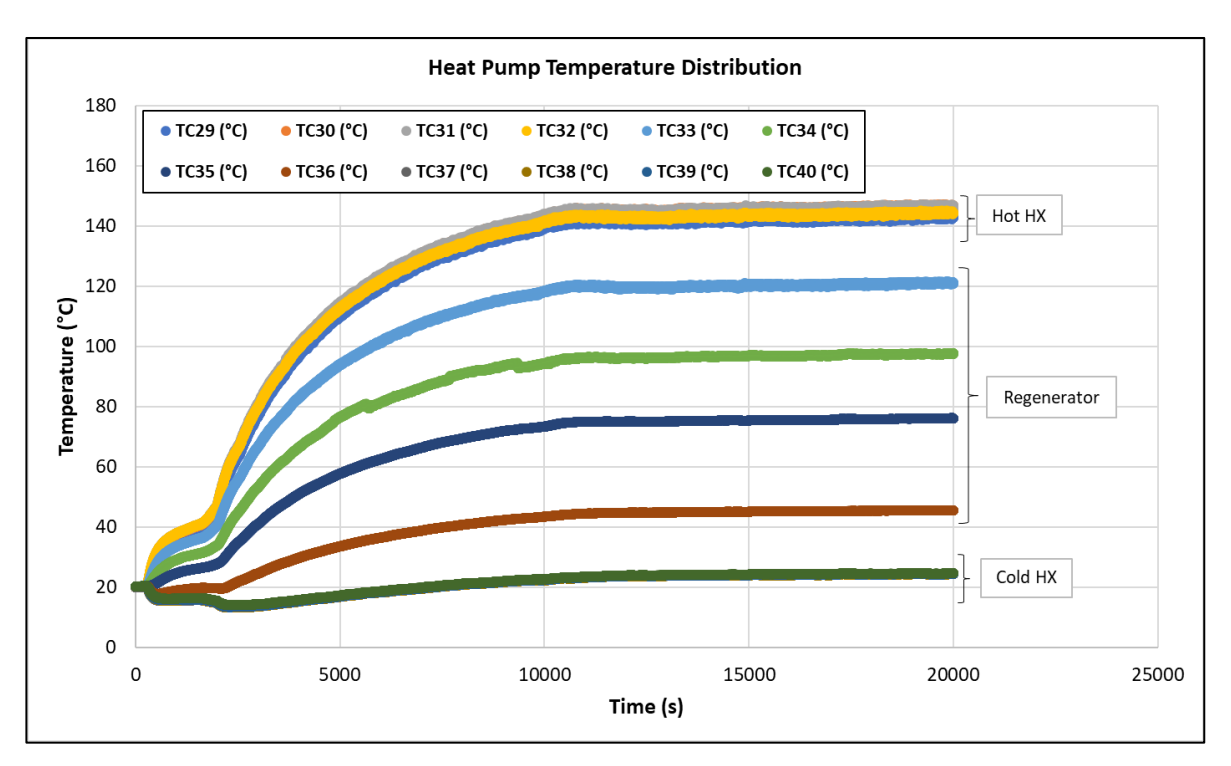


Figure 22. Heat Pump Maximum Power Input From Alternator Thermocouple Data

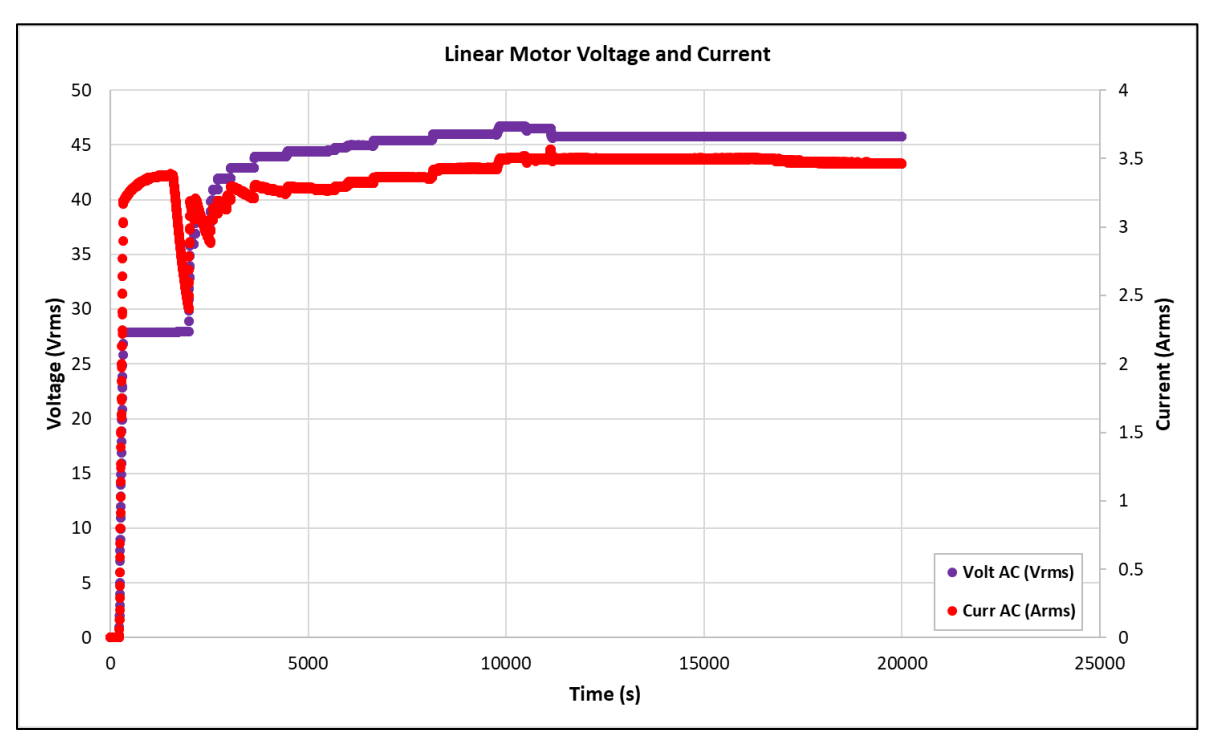


Figure 23. Linear Motor Voltage and Current Data for the Maximum Power Input Test

C. Optical Measurements Utilizing Schlieren System

Figure 24 shows the SA-FS system installed on the TAE. Figure 25 shows the measured density gradient field within the TAHP during operation of the rig, where the optical spool piece is located just downstream of the regenerator in the rig. Hence, the Helium gas is cooled by the regenerator, yielding density gradients in the gas. The image of the flow through the TAE appears to be slightly elliptical, which is caused by some of the light rays near the top and bottom of the glass tube being refracted outside of the glass tube. The light rays nearly tangent to the top and bottom of the tube get refracted into the glass and are totally internally reflected, yielding the clipping observed in the SA-FS images. Figure 26 shows the results from using the density gradients in a sequential pair of SA-FS images from the TAHP as flow tracers to compute the convective flow velocity using techniques commonly employed in Direct Image Correlation (DIC). The flow field within the TAHP is observed to oscillate back and forth, but not in phase with the acoustic waves in the rig. In Sage, a mean velocity profile with an amplitude of 2.4 m/s is computed with in the optical spool section, and it is shown in Figure 27. The Sage velocity amplitude falls within the bounds of the convective velocity measurements shown in Figure 26.

A Proper Orthogonal Decomposition (POD) was performed on the processed velocity vector maps computed from the TREES system using the LaVision DaVis FlowMaster software. A sequence of 4000 vector maps was used as the input to the POD. There is no net flow inside of the TAHP, hence, it is essentially a zero-mean flow, as depicted by the average velocity magnitude in Figure 28. The first temporal mode output from the POD, which should be the most prominent time dependent feature, shows a sinusoidal signal, see Figure 29a. The complex magnitude of the FFT of the first temporal mode is shown in Figure 29b, which shows a sharp peak at 60Hz, which exactly matches the TAHP piston driving frequency. The result from the POD further confirms that the flow inside of the TAHP is dominated by the piston driving frequency.



Figure 24. SAFS System Looking Through the Optical Spool Piece Installed on the TAHP

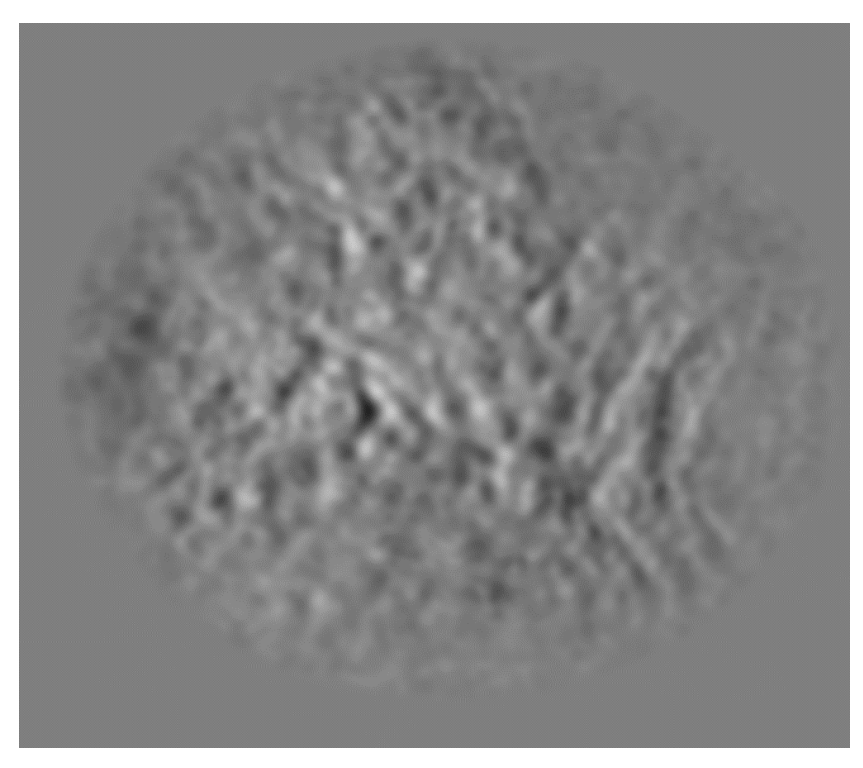


Figure 25. Sample Image of the Density Gradient Field within the TAHP

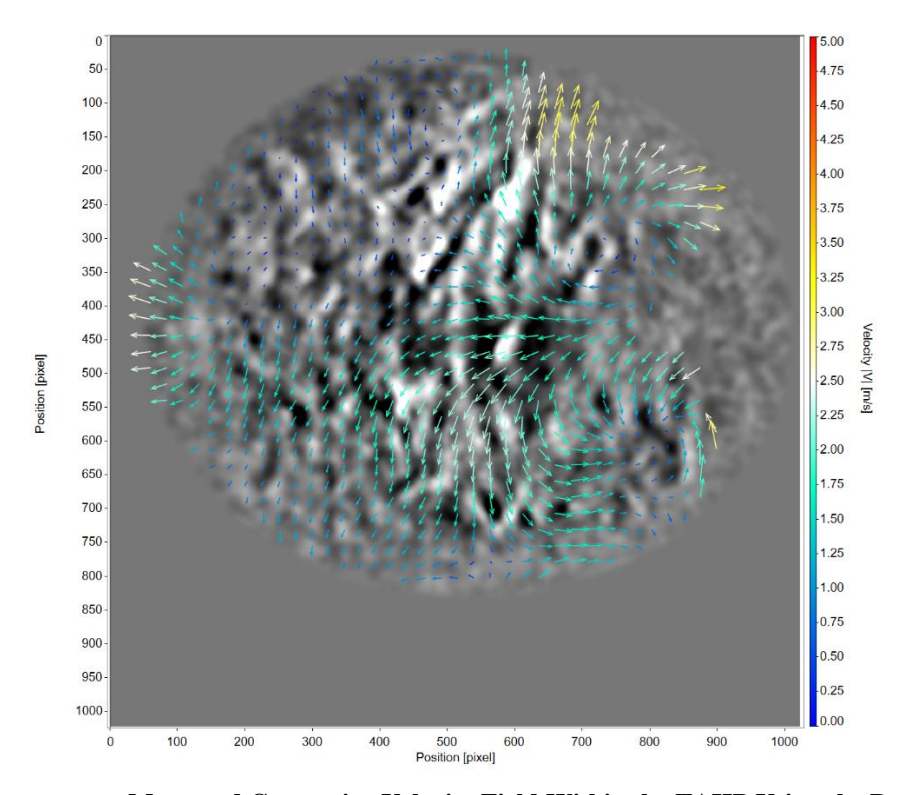


Figure 26. Instantaneous Measured Convective Velocity Field Within the TAHP Using the Density Gradients as the Flow Markers.

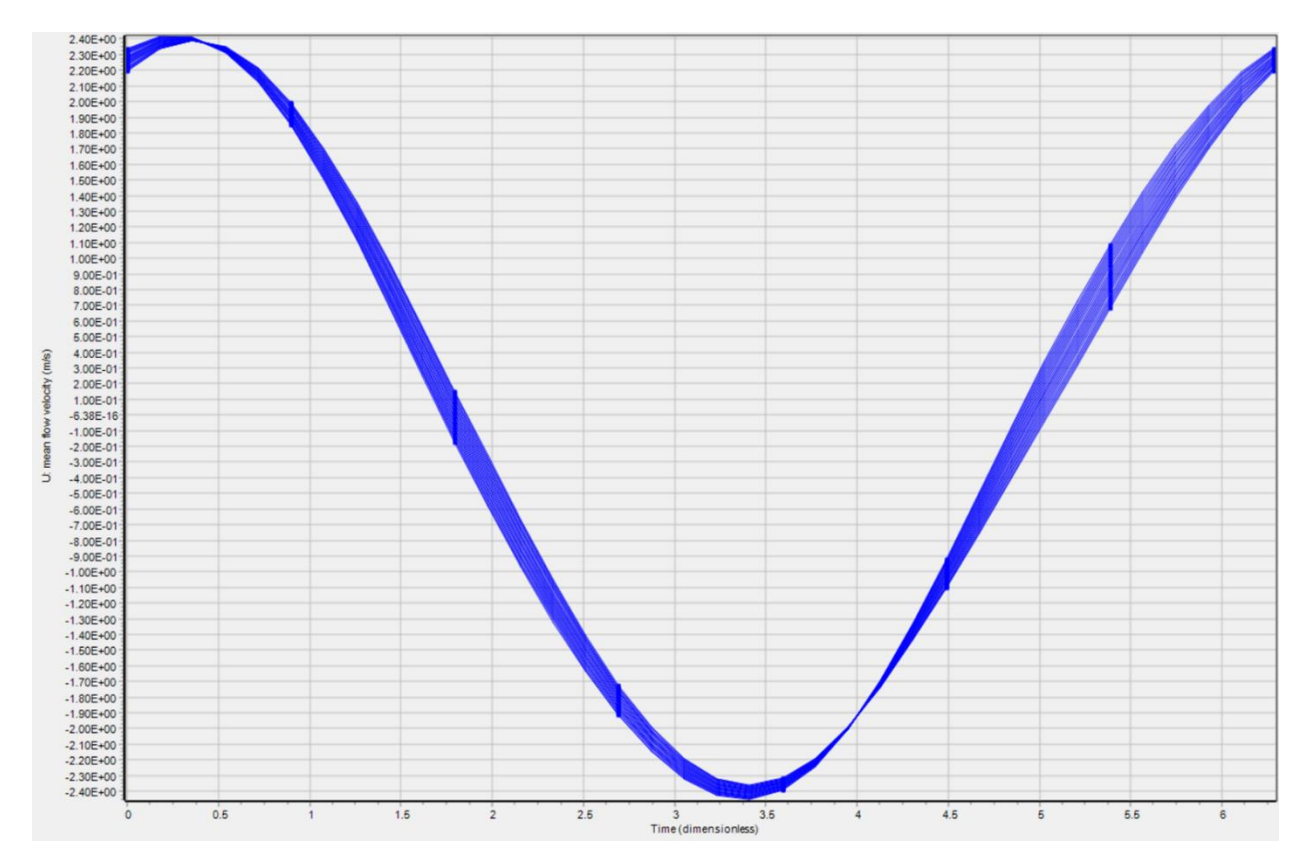


Figure 27. Sage Mean Velocity at Optical Spool Location

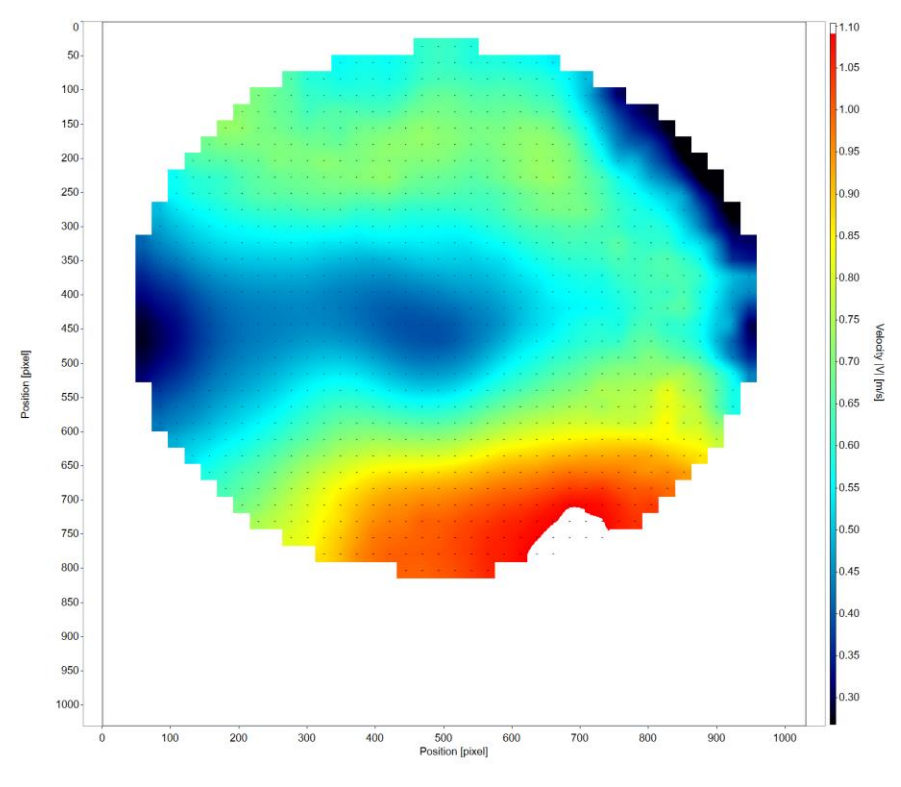
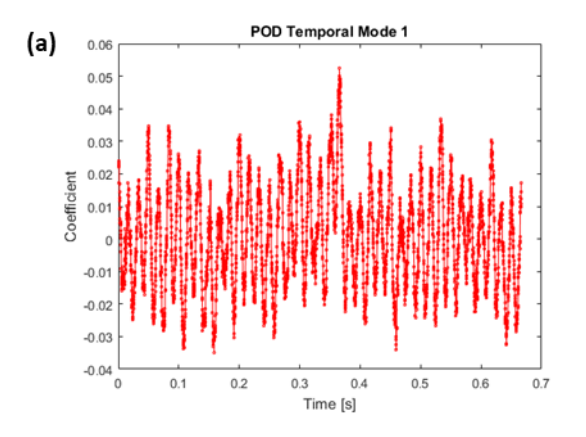


Figure 28. Average Velocity Field Inside the TAHP. Net Velocity Not Shown



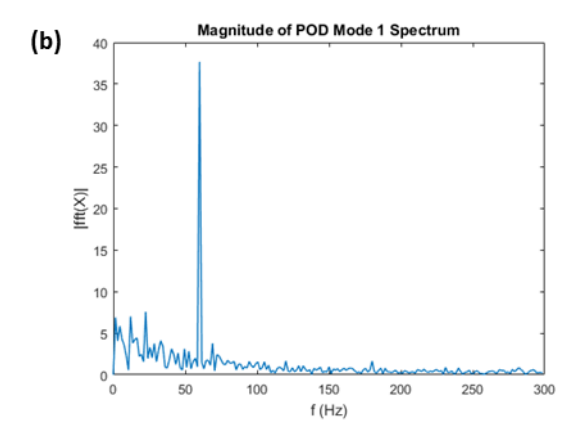


Figure 29. (a) First Temporal Mode from the POD Decomposition of the Velocity Record; B) Complex Magnitude of the FFT Temporal Mode, Showing A Peak At 60Hz.

VII. Summary

Traveling wave systems such as TREES offer several advantages, stemming from their ability to efficiently transport and utilize thermal energy. Some of these advantages are exergy amplification, efficient heat transport, dynamic heat redirection, improved system efficiency, solid-state operation, and versatility. For example:

- Exergy Amplification: Traveling wave systems can effectively increase the exergy (useful energy) by reusing normally wasted high-grade waste heat.
- **Efficient Heat Transport**: The acoustic waves generated in traveling wave systems provide an efficient means of transporting thermal energy throughout a system. This is particularly advantageous in applications like aircraft, where heat sources and sinks are often distributed over considerable distances.
- **Dynamic Heat Redirection**: Traveling wave systems, when combined with dynamically switchable heat pipes, allow for precise control overheat flow and destination.
- **Improved System Efficiency:** By effectively utilizing waste heat and reducing reliance on active cooling methods, traveling wave systems can contribute to overall system efficiency improvements.
- **Solid-State Operation:** Traveling wave systems can be designed with minimal or no moving parts. This translates to increased reliability, reduced maintenance requirements, and longer operational life compared to conventional thermal management solutions.
- **Versatility:** Traveling wave systems can accommodate various heat sources and sinks, making them adaptable to diverse applications.

In this study, TREES was successfully modeled and fabricated at NASA GRC to demonstrate a TMS solution for electric aircraft. TREES demonstrated the ability to convert mechanical energy to acoustic over various distances, with minimal energy dissipation. Also, amplification of acoustic energy is successfully shown in this paper. Furthermore, a Schlieren system along with an optical spool was utilized to study the traveling wave dynamics. This testbed along with the optical system has the potential to serve as a diagnostics tool for future TAHP development.

Acknowledgments

The authors would like to express their gratitude and appreciation to Don Fong, Casey Theman, Frank Lam, Frank Gaspare, and David Hausser for their immense support and resources throughout this research. The authors would also like to thank ACT for their successful work on the TREES full-scale fabrication and testing. Lastly, thanks are extended to Dr. Lee Mears for his assistance and helpful insights into the POD analysis. This work was sponsored by the Advanced Air Transportation Technologies project/Electric Aircraft Powertrain Technologies sub-project.

References

- [1] Chapman, J.W., Schnulo, S.L., and Nitzsche, M.P., "Development of a Thermal Management System for Electrified Aircraft," AIAA 2020-0545. AIAA Scitech 2020 Forum. January 2020.
- [2] Gieras, J.F., "Multimegawatt Synchronous Generators for Airborne Applications: a Review," IEEE International Electric Machines & Drives Conference, Chicago, IL, May 12–15, 2013.
- [3] Dyson, R.W., Rodriguez, L., and Roth, M., Raitano, P., "Solid-State Exergy Optimized Electric Aircraft Thermal and Fault Management," AIAA 2020-3576. AIAA Propulsion and Energy 2020 Forum. August 2020.
- [4] Dyson, R, W., "True Zero Emission Electric Aircraft Propulsion Transport Technology," AIAA 2023-3987. AIAA AVIATION 2023 Forum, June 2023.
- [5] Diebold, J. M., Lee, K., Tarau, C., and Anderson, W.G., "Development of Solid-State Waste Heat Delivery System for Electric Aircraft." 2021 20th IEEE Intersociety Conference on Thermal and Thermomechanical Phenomena in Electronic Systems (iTherm), 2021, pp. 460-466.
- [6] Abdelmaksoud, R., Diebold, J., Ahmed, Z., Leitherer, B., Tarau, C., Lee, K., and Dyson. R., "Status of Development of a Solid-State Thermal Management System of a MW-Scale Electric Aircraft," AIAA 2024-2364. AIAA SCITECH 2024 Forum, Jan. 2024.
- [7] Van Heerden, A. S. J., Judt, D. M., Jafari, S., Lawson, C. P., Nikolaidis, T., & Bosak, D. (2022). "Aircraft thermal management: Practices, technology, system architectures, future challenges, and opportunities," *Progress in Aerospace Sciences*, Vol. 128, Jan. 2022, 100767.
- [8] Feldman, K.T., "Review of the literature on Sondhauss thermoacoustic phenomena", *Journal of Sound and Vibrations*, Vol.7, Jan. 1968, pp. 71-72.
- [9] Ceperley, P.H., "A pistonless Stirling engine—The traveling wave heat engine", *J. Acoust. Soc. Am.* Vol. 66, Nov 1979, pp. 1508–1513.
- [10] Swift, G. W., Thermoacoustics: A Unifying Perspective for Some Engines and Refrigerators, Springer, 2017
- [11] McGaughy, M., Wang, C., Boessneck, E., Salem, T., and Wagner, J., "A Traveling Wave Thermoacoustic Engine—Design and Test." *ASME. Letters Dyn. Sys. Control.*, Vol 1, July 2021, 031006
- [12] Sage, Ver. 12, Gedeon Associates, Athens, OH, 2021.
- [13] Bathel, B. F., and Weisberger, J. M., "Development of a Self-Aligned Compact Focusing Schlieren System for NASA Test Facilities", AIAA SciTech 2022 Forum, AIAA-2022-0560.